Non-equilibrium plasma kinetics of reacting CO: an improved state to state approach

L. D. Pietanza*, G. Colonna and M. Capitelli

CNR NANOTEC, P.Las.M.I. Lab
Via Amendola 122/D, 70126 Bari, Italy

*corresponding author: luciadaniela.pietanza@cnr.it

Abstract

Non-equilibrium plasma kinetics of reacting CO for conditions typically met in microwave discharges has been developed based on the coupling of excited state kinetics and the Boltzmann equation for the electron energy distribution function (eedf). Particular attention is given to the insertion in the vibrational kinetics of a complete set of electron molecule resonant processes linking the whole vibrational ladder of the CO molecule, as well as to the role of Boudouard reaction, i.e. the process of forming CO_2 by two vibrationally excited CO molecules, in shaping the vibrational distribution of CO and promoting reaction channels assisted by vibrational excitation (pure vibrational mechanisms, PVM). PVM mechanisms can become competitive with electron impact dissociation processes (DEM) in the activation of CO.
A case study reproducing the conditions of a microwave discharge has been considered following the coupled kinetics also in the post discharge conditions.
Results include the evolution of eedf in discharge and post discharge conditions highlighting the role of superelastic vibrational and electronic collisions in shaping the eedf. Moreover, PVM rate coefficients and DEM ones are studied as a function of gas temperature, showing a non-Arrhenius behavior, i.e. the rate coefficients increase with decreasing gas temperature as a result of a vibrational-vibrational (V-V) pumping up mechanism able to form plateaux in the vibrational distribution function (VDF).
The accuracy of results is in particular discussed in connection to the present knowledge of the activation energy of the Boudouard process.

1 Introduction

Large attention is presently devoted to the activation of CO_2 by non-equilibrium plasmas, leading to the dissociation process

$$CO_2(00v) + M = CO + O + M \qquad (1.1)$$

Different plasma sources are used to reach this goal including microwave MW [1], DBD [2, 3], repetitive nano-pulsed (NPD) [4] and gliding arc discharges [5, 6]. In these kinds of plasmas, the initial CO_2 component is transformed in a complex mixture where the CO molecule can result the majority component. In these conditions, the vibrational kinetics of CO should be treated with the same attention devoted to that one of CO_2 [7-10]. This aspect is also important for CO plasmas used in the last years for the production of nanostructures [11, 12].
At the moment, the most complete CO_2/CO plasma chemistry model [13-15] has considered up to 63 vibrational levels of CO [14], limiting them to the first 10 levels in later papers to reduce computational times. This approximation, good for some applications, cannot be used when the vibrational distributions of non-equilibrium plasma conditions present long plateau which, contrary to the CO_2, have been experimentally detected [16, 17]. Moreover, the CO system presents well defined metastable electronic states, which can affect the electron energy distribution function (eedf) through the corresponding superelastic collisions [18], a problem also met in CO_2 discharges [7-10].
These preliminary considerations justify a re-examination of the CO kinetics under non-equilibrium plasma conditions, improving the model developed some years ago in the present laboratory [19, 20] applied only to discharge conditions. In this context, an attempt to face some of the problems still existing in the kinetics of CO plasmas is carried out including the investigation of 1) the role of a complete set of resonant electron-impact cross sections (e-V) coupling the whole vibrational ladder of CO in competition with the classic V-V (vibration-vibration) and V-T (vibration-translation) energy transfer processes 2) the role of Boudouard reaction in affecting reaction rates, vibrational distribution and eedf in the CO system.
In both cases, we will take into account the recent developments present in literature, in particular, the ab-initio calculation of resonant e-V cross sections of CO performed by Laporta et al. [21, 22] and the quantum mechanical derivation of the activation energy of the Boudouard reaction performed by Barreto et al [23].
To show the similarity between CO and CO_2 discharges, we select typical electrical conditions considered for the MW case of a CO_2 plasma in [8-10]. The results will be presented as in the CO_2 case emphasizing the role of pure vibrational mechanisms in activating CO as compared with the corresponding electron impact dissociation processes. Moreover, the role of superelastic vibrational and electronic collisions in affecting eedf will be reported anticipating the possible role of these processes when the CO kinetics will be linked to the corresponding CO_2 one. Note, however, that the present study does not consider the V-V' energy transfer between the formed CO_2 by the Boudouard reaction and the CO vibrational distribution. This point, while justified by the small concentrations of CO_2 found in the present study, should be considered for the CO_2/CO mixtures when the concentration of CO_2 is the main component.
The paper is organized in different sections. After the introduction, section 2 reports the kinetic model detailing the vibrational and electronic states and their cross sections, the vibrational and electronic kinetics and their coupling with the

Boltzmann equation; section 3 reports the results following the same philosophy of those discussed for CO_2 emphasizing their dependence on gas temperature in particular the non-Arrhenius behavior of the rate coefficients [10, 24, 25] and on the reduced electric field E/N. Finally, section 5 reports the conclusions.

2 The model

The model is based on the solution of a zero-dimensional time dependent Boltzmann equation for the electrons coupled to the non-equilibrium vibrational and electronic excited state kinetics of CO molecule, as well as, with a simple dissociation and ionization kinetics describing the plasma mixture [8-10].
The electron Boltzmann equation takes into account the effect of the applied electric field, elastic electron-molecule, electron-electron, inelastic and superelastic (vibrational and electronic) collisions [26, 27]. The plasma mixture considered is composed of the following species: CO, CO_2, C, O, CO^+, CO_2^+, C^+, O^+ and e^-.
At this stage, the CO_2 molecule (and also all the ions, CO^+, CO_2^+, C^+ and O^+) is considered only in its ground state and its vibrational kinetics, deeply investigated in our recent papers [7-10], is neglected. This assumption can be justified by the small concentrations of CO_2 formed in pure CO discharges at least for the conditions studied in the present paper. Only in a future improvement of the model, the vibrational kinetics of CO and CO_2 will be coupled by taking into account the vibrational-vibrational (V-V') energy exchange processes between the two vibrational ladders.

2.1 Energy level diagrams

The energy level diagrams of CO, C and O are schematically represented in Fig. 1. The CO molecule has 80 vibrational levels in the ground electronic state ($X^1\Sigma^+$), whose energies, calculated in the anharmonic oscillator approximation, have been taken from the work [21], together with the dissociation energy value of 11.128 eV (CO $\rightarrow$C(^{3}P)+O(^{3}P)). Besides the ground state, the CO molecule presents several electronic excited states, divided into singlet and triplet state according to their spin degeneracy. The following seven electronic excited states are included in the model: three triplet states, $a^3\Pi$ (6.006 eV), $a'^3\Sigma^+$ (6.863), $b^3\Sigma^+$ (10.40 eV) and four singlet states, $A^1\Pi$ (8.03 eV), $B^1\Sigma^+$ (10.78 eV), $C^1\Sigma^+$ (11.40 eV), $E^1\Sigma^+$ (11.52 eV).
For C and O atoms, only four and five electronic levels are accounted, see Fig. 1 b, which from now on will be labeled as C(^{3}P), C(^{1}D), C(^{1}S), C(^{5}S^0) and O(^{3}P), O(^{1}D), O(^{1}S), O(^{3}S) and O(^{5}S), respectively. Their energies have been taken from the NIST database.

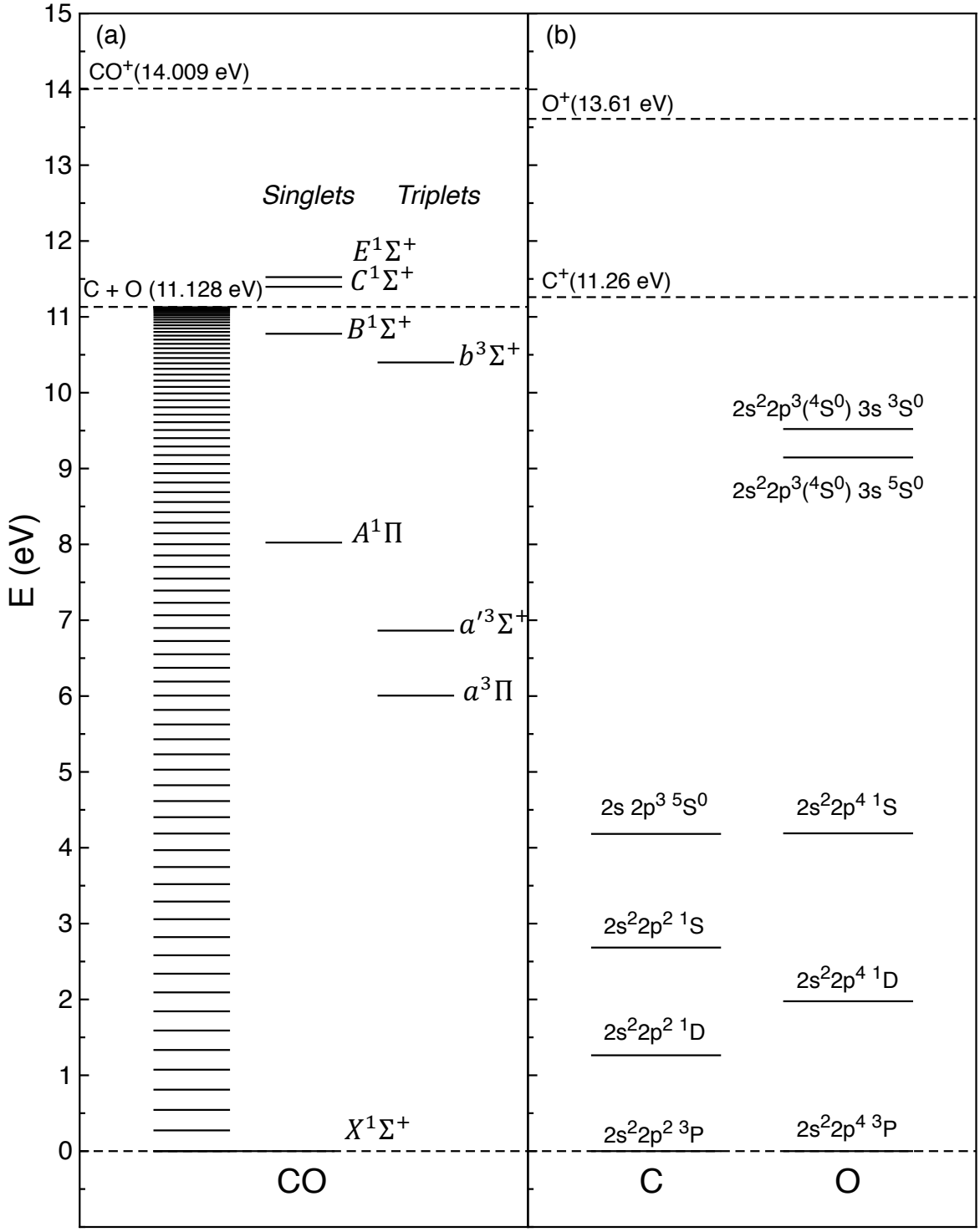

Fig. 1 Schematic representation of the (a) CO and (b) C and O energy level diagrams.

2.2 Electron impact cross sections for the Boltzmann equation

The electron impact cross sections entering in the Boltzmann equation are those corresponding to the processes listed in Table 1. For all the plasma species (CO, CO_2, C, O, $CO^{+,}$ C^+, O^+) momentum transfer cross sections (MT), taken mainly from the LXCat database [28], are accounted. For the CO molecule, the cross sections for

ionization from ground state ($I_{CO}(0)$) and for excitation from ground state of the excited states (Met_{CO}) are accounted and the corresponding cross sections have been taken from the Itikawa database [29]. The direct dissociation cross section from ground state ($D_{dir}(0)$), instead, is the experimental Cosby one [30] with threshold energy 13.5 eV. The cross sections for ionization ($I_{CO}(v)$) and dissociation ($D_{dir}(v)$) from each vibrational level of CO have been estimated from the corresponding ground state cross sections by shifting the threshold energy according to the vibrational energy of the level, without changing the modulus of the cross sections.
Resonant vibrational excitation cross sections (e-V_{Res}) and resonant dissociation cross sections (D_{Res}) for the whole CO vibrational ladder have been taken into account for the first time in a state-to-state CO kinetic model. In these processes, the incident electron is attached to form a temporary negative ion CO^- and then vibrational excitation or dissociation is induced. Laporta et al. [21, 22] provided the complete set of vibrational state-resolved cross sections for all the vibrational levels of the ground electronic excited state of CO, which are strongly state-dependent (v_i, v_f). In particular, resonant vibrational excitation cross sections are characterized by resonance spikes, whose width is related to the lifetime of the unstable, intermediate, negative ion vibrational level of $CO^-(\,^2\Pi)(v_{int})$ and the maximum value of the cross sections at fixed v_i usually decreases with the increase of the final vibrational number v_f (mono-quantum transitions are more probable than multi-quantum ones). Resonant dissociation cross section from v=0 is very small but it increases rapidly for higher vibrational levels.
For C and O atoms, ionization cross sections from C(^{3}P) (I_C and I_O) and excitation cross sections linking few electronic levels are accounted (e-C and e-O) and the cross section taken respectively from [31] for C and [32] for O.

Table 1. Electron impact processes

Process	Label	Reference
$e + X \leftrightarrow e + X, X = CO, CO_2, C, O, CO^+, C^+, O^+$	MT	[28][20]
$e + CO(0) \leftrightarrow e + CO^+ + e$	$I_{CO}(0)$	[29]
$e + CO(v) \leftrightarrow e + CO^+ + e$	$I_{CO}(v)$	[29]
$e + CO(0) \leftrightarrow e + CO(X)$, $X = a^3\Pi, a'^3\Sigma^+, b^3\Sigma^+, A^1\Pi, B^1\Sigma^+, C^1\Sigma^+, E^1\Sigma^+$	Met_{CO}	[29]
$e + CO(0) \leftrightarrow e + C + O$	$D_{dir}(0)$	[30]
$e + CO(v) \leftrightarrow e + C + O$	$D_{dir}(v)$	[30]
$e + CO(\,v_i) \rightarrow CO^-(\,^2\Pi) \rightarrow e + CO(v_f)$	e-V_{Res}	[22]
$e + CO(\,v_i) \rightarrow CO^-(\,^2\Pi) \rightarrow e + C(\,^3P) + O(\,^3P)$	D_{Res}	[21]
$e + C(\,^3P) \leftrightarrow e + C^+$	I_C	[31]
$e + O(\,^3P) \leftrightarrow e + O^+$	I_O	[32]
$e + C(\,^3P) \leftrightarrow e + C(X), X = \,^1D,\ ^1S,\ ^5S^0$	e-C	[31]
$e + O(\,^3P) \leftrightarrow e + O(X), X = \,^1D,\ ^1S,\ ^3S^0,\ ^5S^0$	e-O	[32]

2.3 CO plasma chemistry

2.3.1 Pure vibrational mechanisms

The Pure Vibrational Mechanisms for CO considers two different reactive channels assisted by vibrational excitation:

1) Direct dissociation (PVM_1)

$$CO(v) + M \rightarrow C + O + M \qquad (2.3.1)$$

2) Boudouard or disproportionation reaction (PVM_2)

$$CO(v) + CO(w) \rightarrow CO_2 + C \qquad (2.3.2)$$

The first PVM mechanism is given by direct dissociation in which the CO molecule in the vibrational state v by colliding with another molecule that could be CO, C, O or CO_2 dissociates producing C and O atoms. The corresponding rate coefficient from ground state has been taken from [33] and described by the following Arrhenius expression

$$K_{v=0} = AT^{\eta} \exp(-\theta/T) \qquad (2.3.3)$$

with $A = 1.74\ 10^{-9}\ cm^3 s^{-1}, \eta = 0.19,\ \theta = 123661$ K. The rate coefficients of dissociation process from all the vibrational level of CO have been calculated according to the Fridman-Macheret *alpha*-model [34], as already done for CO_2 [2, 8, 9]. According to this model, the vibrational energy lowers the activation energy of the chemical reactions according to the following law,

$$K_d^{direct}(v) = K_{v=0} \exp(\alpha E_v/T) \qquad (2.3.4)$$

where α is a parameter that determines the efficiency of vibrational energy in lowering the reaction barrier. It should be noted that, when $\alpha E_v \geq \theta$, $K_d^{direct}(v) = K_{v=0}$. According to Macheret and Fridman rules, α=1 for strongly endothermic reactions, as in the case of reaction (2.3.1).
The other mechanism of PVM dissociation is called Boudouard or disproportionation process (see eq. (2.3.2)) in which two vibrational excited CO molecules react forming CO_2 and C.
The corresponding state specific rate coefficient can be written in the following way [17, 19, 34]

$$k_D^{Boud}(v,w) = k_g \sqrt{\frac{T}{300}} \cdot S \cdot A_{vw} \cdot f_v f_w \left[1 - \frac{E_a}{E_v + E_\omega}\right]^2 \left(\frac{\omega_{CO}}{\omega_{CO_2}}\right)^2 \qquad (2.3.5)$$

where $k_g = 3\times10^{-10} cm^3 s^{-1}$ is the gas kinetic rate at room temperature, T the gas temperature, $S \leq 1$ the steric factor, A_{vw} the step function

$$A_{vw} = \begin{cases} 1, \ if \ E_v + E_\omega \geq E_a \\ 0, \ if \ E_v + E_\omega < E_a \end{cases} \qquad (2.3.6)$$

with E_v ed E_ω the vibrational energies of the two CO molecules, E_a the reaction activation energy, f_v and f_ω the normalized CO vibrational level populations, $\omega_{CO} = 2214.24 \ cm^{-1}$ and $\omega_{CO_2} = 2226.85 \ cm^{-1}$ the vibrational quanta of CO and of CO_2 asymmetric mode.
The formed C and O atoms, produced also by electron impact dissociation processes are allowed to recombine according to the process

$$C + O + M \rightarrow CO + M \qquad (2.3.7)$$

the rate coefficient of the process, taken from [13], is

$$2.14 \ 10^{-29} (T/300)^{-3.08} exp(-2114/T) \ \text{cm}^6/\text{s} \qquad (2.3.8)$$

2.3.2 Ionization kinetics

Electron impact ionization is considered occurring by the following channels

$$e + CO(v) \leftrightarrow e + CO^+ + e \qquad (2.3.9)$$

$$e + C(\ ^3P) \leftrightarrow e + C^+ \qquad (2.3.10)$$

$$e + O(\ ^3P) \leftrightarrow e + O^+ \qquad (2.3.11)$$

Their rate coefficients are calculated by integrating the product of the corresponding cross sections, used for the Boltzmann equation (see Table 1), the electron velocity and the eedf over the electron energy.
Ion losses occur mainly by the dissociative recombination process

$$CO^+ + e \rightarrow C + O \qquad (2.3.12)$$

2.4 CO vibrational kinetics

The CO vibrational distribution function (VDF) is obtained by the solution of the following coupled system of differential equations, one equation for each vibrational level,

$$\frac{dN_v}{dt} = \left(\frac{dN_v}{dt}\right)_{e-V} + \left(\frac{dN_v}{dt}\right)_{e-D} + \left(\frac{dN_v}{dt}\right)_{e-I} + \left(\frac{dN_v}{dt}\right)_{PVM} + \left(\frac{dN_v}{dt}\right)_{V-V} + \left(\frac{dN_v}{dt}\right)_{V-T} + \left(\frac{dN_v}{dt}\right)_{SE} \quad (2.4.1)$$

where e-V, e-D and e-I contributions correspond, respectively, to the electron-impact resonant vibrational excitation processes (e-V_{Res}), to the two contributions of direct (D_{Dir}) and resonant (D_{Res}) dissociation processes and to ionization (I_{CO}) processes listed in Table 1. The PVM term corresponds to the contribution of dissociation induced by vibrational excitation due to both direct dissociation (eq. 2.3.1) and the Boudouard process (eq. 2.3.2). The last terms (V-V, V-T and SE) correspond to the following energy-exchange processes:

1) V-V (vibration-vibration)

$$CO(v) + CO(w) \leftrightarrow CO(v-1) + CO(w+1) + \Delta\varepsilon \quad (2.4.3)$$

2) V-T (vibration-translation) by CO

$$CO(v) + CO \leftrightarrow CO(v-1) + \mathrm{CO} + \Delta\varepsilon_T \quad (2.4.4)$$

3) V-T by C, O

$$CO(v) + C \leftrightarrow CO(v-1) + \mathrm{C} + \Delta\varepsilon_T \quad (2.4.5)$$
$$CO(v) + O \leftrightarrow CO(v-1) + \mathrm{O} + \Delta\varepsilon_T \quad (2.4.6)$$

4) SE (spontaneous emission)

$$CO(v) \leftrightarrow CO(w) + h\nu_{vw} \quad (2.4.7)$$

The rate coefficients of the V-V (eq. 2.4.3) and V-T by CO (eq. 2.4.4) processes have been taken from the works [35, 36] in the framework of the forced harmonic oscillator approximation (FHO). The corresponding rate coefficients are in satisfactory agreement with the results obtained by semi-classical calculation by Cacciatore and Billing [37].
Besides the V-T processes by CO molecules, a strong contribution to the CO vibrational kinetics is given by the VT deactivation by O and C atoms (eq. 2.4.4), whose rate coefficients have been taken from [19, 38].
Spontaneous emission processes (see eq. (2.4.7)) for the fundamental, first and second overtone transitions of the first 30 vibrational levels of CO have been also included [39].
Fig. 2 shows the resulting V-V and V-T rate coefficients as a function of the vibrational level at a fixed gas temperature of 500 K.

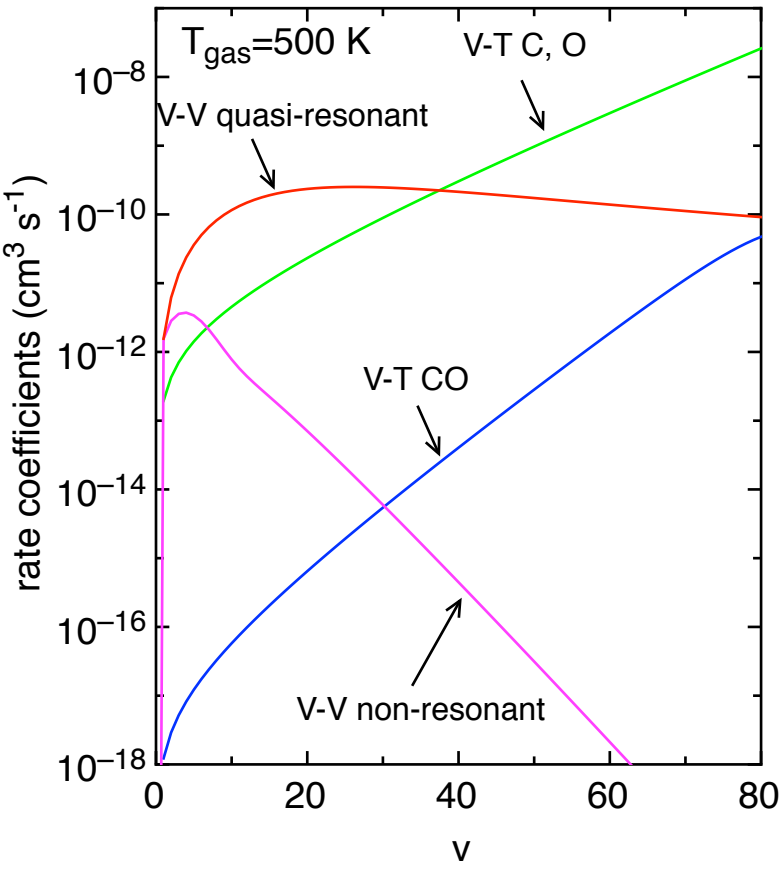

Fig. 2 V-V quasi-resonant, V-V non-resonant, V-T by CO and C, O rate coefficients at T_{gas}=500 K as a function of the vibrational quantum number v.

In particular, we have reported V-V rate coefficients of the quasi-resonant process of the kind

$$CO(v) + CO(v) \rightarrow CO(v-1) + CO(v+1) \qquad (2.4.8)$$

and of the V-V non-resonant process

$$CO(1) + CO(v) \rightarrow CO(0) + CO(v+1) \qquad (2.4.9)$$

together with the V-T monoquantum transition rate coefficients by C, O and CO. The interplay between V-V and V-T rate coefficients as well as the disproportionation reaction rate coefficients will be responsible of the form of VDF, in particular of the plateau extension in the VDF.

2.5 Boudouard process: activation energy values

The rate coefficient of the Boudouard process depends on the activation energy value (E_a) entering in eq. (2.3.5). The first estimation proposed by Rusanov and Fridman was 6 eV [40]. This value, used by Gorse et al [18], was too low to explain the experimental vibrational distributions reported by De Benedictis et al [16]. Many

years after, Essenigh et al [17] obtained an activation energy of 11.6 eV by an indirect experimental method based on eqs. (2.3.5) and (2.3.6), on the experimentally determined vibrational distribution function of CO and the experimental production of CO_2 in a laser pumped experiment. To justify the very high deactivation energy of 11.6 eV, very near to the dissociation energy of the molecule, Essenigh et al [17] suggested that the reaction proceeds via breaking one of the C-O bonds in the transition state complex. Note that accepting this high value, the Boudouard reaction can occur only in collisions of two very highly vibrationally excited CO molecules.
Very recently, a third estimation of E_a has been proposed by Barreto et al [23], suggesting an intermediate value of 8.3 eV (a similar value of 8 eV was also found by Martin et al [41]). The 8.3 eV value was obtained by a quantum mechanical calculation of the energies of reagents, products and transition state in the reactive path [23]).
Fig. 3 shows the PVM rate coefficients of both direct and Boudouard mechanism (calculated at the three E_a values of 6, 8.3 and 11.6 eV) as a function of the vibrational level at gas temperature equal to 500 K. The rate coefficient of the Boudouard dissociation mechanism and thus its contribution both to global dissociation and to the shape of the CO VDF depend on the value of the chosen activation energy. The lower the activation energy, the higher the disproportionation reaction rate coefficient, the shorter the V-V plateau in the CO VDF. The same trend is expected by the action of carbon atoms, which present very large VT deactivation rate coefficients. In section 3.2, the results obtained by changing the activation energy value of the Boudouard process will be compared and discussed. On the other hand, as it can be seen from Fig. 3, the direct process (PVM_1) is characterized by a higher activation energy and will affect only the tail of the CO VDF distribution (for $v>60$), which, however, will be strongly deactivated by VT processes, thus its net contribution to CO dissociation will be less important than the Boudouard dissociation mechanism.

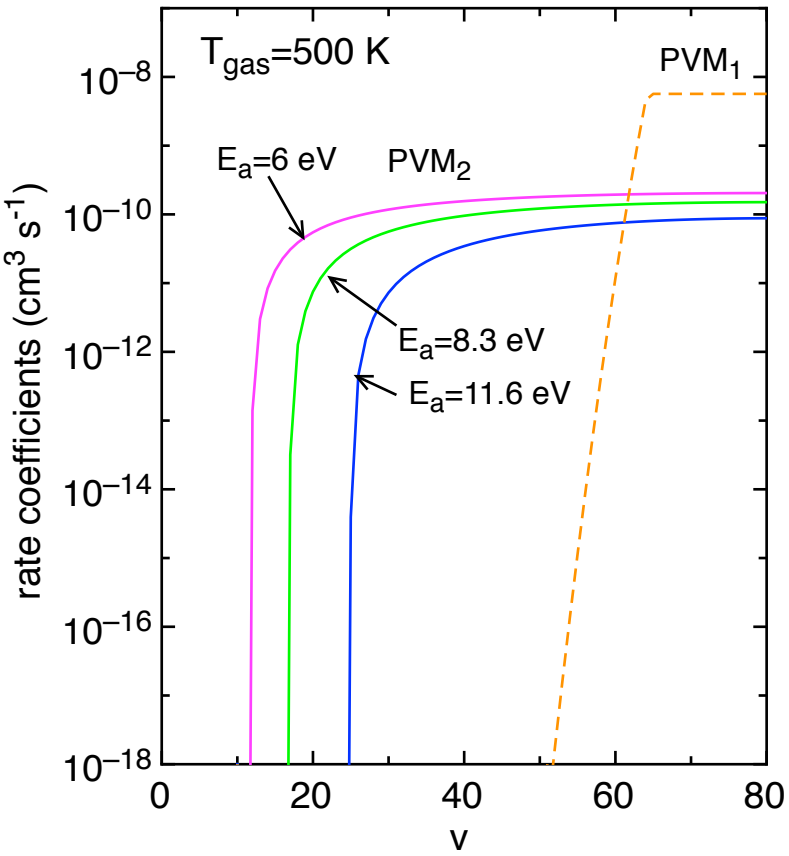

Fig. 3 PVM_1 and PVM_2 rate coefficients at three different activation energies (6, 8.3 and 11.6 eV) at T_{gas}=500 K as a function of the vibrational quantum number v.

3 Results

In this section, the results obtained by applying the self-consistent model to the CO mixture will be presented. In particular, in section 3.1, the results obtained in a MW test case study will be shown. After that, in section 3.2, 3.3 and 3.4 the dependence of VDF, PVM and DEM rate coefficients on, respectively, the activation energy of the Boudouard process (sect. 3.2), the gas temperature (sect. 3.3) and the E/N value (sect. 3.4) will be investigated. Finally, the effect of adding a more refined kinetics of the metastable electronic excited state $a^3\Pi$ will be shown (sect. 3.5).

3.1 MW test case

The MW test case study is characterized by the following values of pressure, gas temperature, pulse duration and reduced electric field value: P=5 torr, T_{gas}=500 K, τ_{pulse}=2.5 ms, E/N=60 Td. At the beginning of evolution (t=0), all CO molecules are in the v=0 level, while the ionization degree is 10^{-6}. In this test case, the intermediate value of 8.3 eV is used for the activation energy of the Boudouard process. The results obtained for a pure CO mixture follow the presentation of pure CO_2 mixture [8-10].

Fig. 4 a and b show, respectively, the time evolution of electron and CO vibrational temperature and of the molar fractions in the test case study.

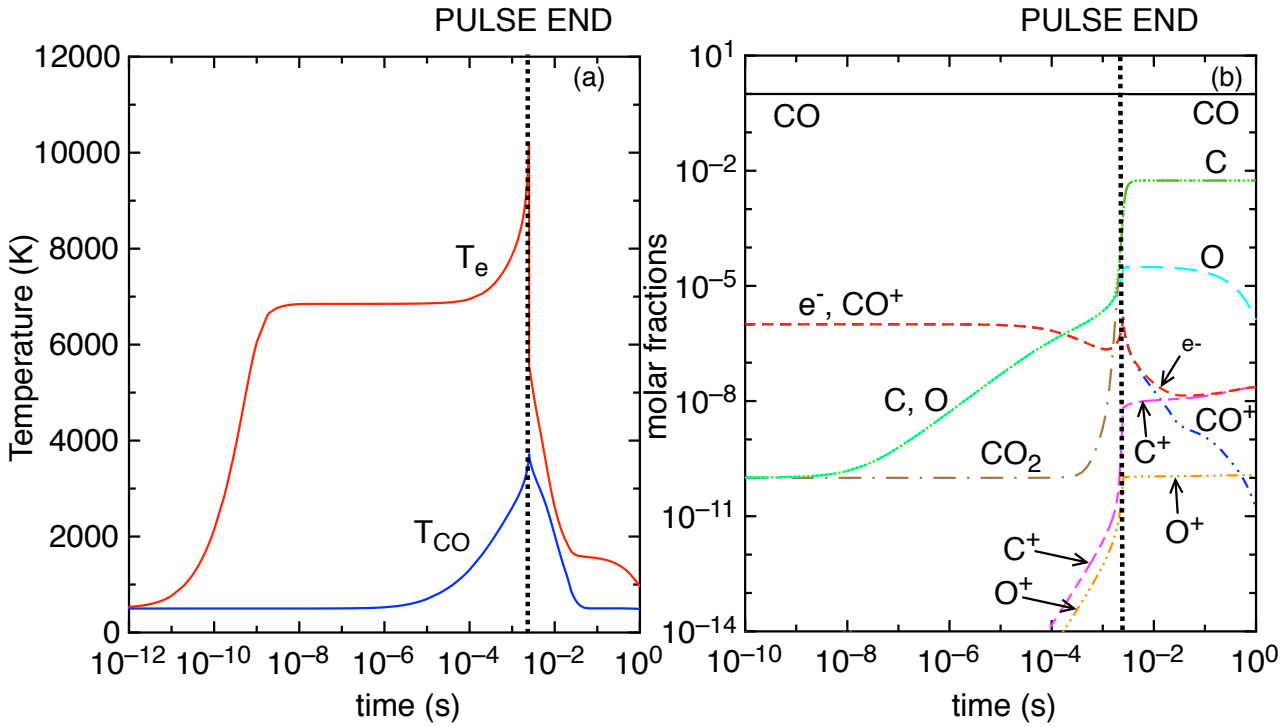

Fig. 4 a and b Time evolution of electron and CO vibrational temperatures (a) and of the molar fractions in the MW test case.

The electron temperature is calculated from the mean electron energy $T_e=2/3*E_{average}$, while the vibrational temperature from the first two levels of the VDF by imposing a Boltzmann distribution. The time dependent behavior is governed by the characteristic e-V, V-V and V-T relaxation times, respectively τ_{e-V}, τ_{V-V} and τ_{V-T} by CO and by C, O. Table 2 shows their estimation performed at the end of the pulse, together with the τ_{eedf}, which represents the characteristic time for reaching quasi-stationary values in the eedf after the reduced electric field is applied. As it can be seen from Table 2 such relaxation times are calculated from the corresponding rate coefficients linking the ground and the first vibrational level.

Table 2 a Characteristic times evaluated at the end of the pulse ($\tau_{pulse} = 2.5\, ms$) from the corresponding rate coefficients linking the ground and the first vibrational level.

τ_{eedf} $= (n_{CO}K_{eV}^{1,0})^{-1}$	τ_{e-V} $= = (n_eK_{eV}^{1,0})^{-1}$	τ_{V-V} $= = (n_{CO}K_{1,0}^{1,0})^{-1}$	$\tau_{V-T\,(CO)}$ $= = (n_{CO}K_{vT(CO)}^{1,0})^{-1}$	$\tau_{V-T\,(C)}$ $= = (n_CK_{vT(C)}^{1,0})^{-1}$
$1.02\ 10^{-9}$ s	$7.33\ 10^{-4}$ s	$6.66\ 10^{-6}$ s	8.46 s	$8.00\ 10^{-2}$ s

The electron temperature increases due to the effect of the electric field and reaches a quasi-stationary condition in times of the order of few nanoseconds (see τ_{eedf} in Table 2). This quasistationary condition corresponds to the cold gas approximation, i.e. when the vibrational distribution is not appreciably populated. Only on longer

time scale (τ_{e-V}), e-V processes are able to transfer energy into the vibrational ladder, increasing the vibrational temperature as well. The quanta introduced into the vibrational ladder are very soon redistributed among the vibrational ladder on the time scale τ_{V-V}, forming the V-V plateau. Once the vibrational temperature is sufficiently high, superelastic vibrational collisions of the kind

$$e^-(\varepsilon) + CO(v) \rightarrow e^-(\varepsilon + \Delta_{vw}) + CO(w) \qquad (3.1.1)$$

with v>w and $\Delta_{vw} = E_v - E_w$, are responsible of the further increase of the electron temperature just before the pulse end. The CO vibrational temperature reached at the end of the pulse is comparable to that obtained in the MW test case of pure CO_2 [8-10]. When the pulse is turned off, the electron temperature suddenly decreases and consequently also the vibrational temperature start decreasing. At much longer times, the vibrational temperature and the electron temperature, relax toward the gas temperature due to V-T deactivation processes firstly by C and O atoms, occurring on a shorter time scale (see $\tau_{V-T(C)}$) and later by CO ($\tau_{V-T(CO)}$) (see Table 2).

The time evolution of molar fraction shows that, at these conditions, the CO dissociation is small and that the prevalent dissociation mechanism is the Boudouard process leading to higher concentration of C and CO_2 than O one, after the pulse. Electron molar fraction does not appreciably change during the discharge, while it firstly decreases of nearly two order of magnitude in the post discharge due to dissociative recombination of CO^+, reaching later a stationary value linked to the ionization of C atoms.

Fig. 5 a and b show the CO VDF in discharge (a) and post-discharge (b) conditions.

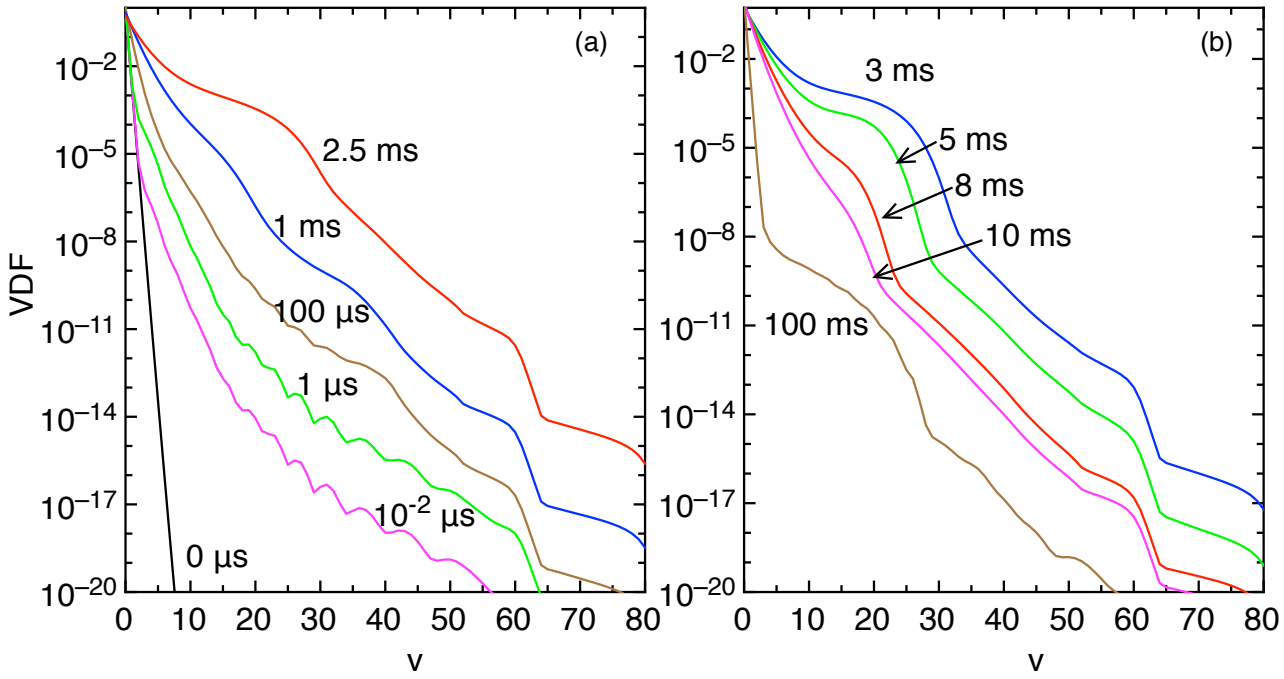

Fig. 5 a and b CO VDF as a function of the vibrational quantum number v during the discharge (a) and the post-discharge (b) in the MW test case.

During the discharge, the VDF is heated as a result of e-V processes acting over all the vibrational ladder and by V-V processes. At the end of pulse (τ_{pulse}=2.5 ms), a plateau appears extending up to v=30 as a result of V-V processes. The plateau is maintained in the post discharge up to 5 ms starting to be deactivated from 8 ms on. The length of the V-V plateau depends on the competition between V-V up-pumping mechanism and the most relevant deactivation processes in CO plasma, the Boudouard process and the V-T deactivation by C and O atoms. By changing the activation energy of the Boudouard dissociation process, the depletion zone will move and the length of the plateau will change: the higher the activation energy, the longer the V-V plateau.
Fig. 6 a and b, instead, show the corresponding EEDF time evolution in discharge (a) and post-discharge (b) conditions. The corresponding Boltzmann solver is discussed by [7-10].

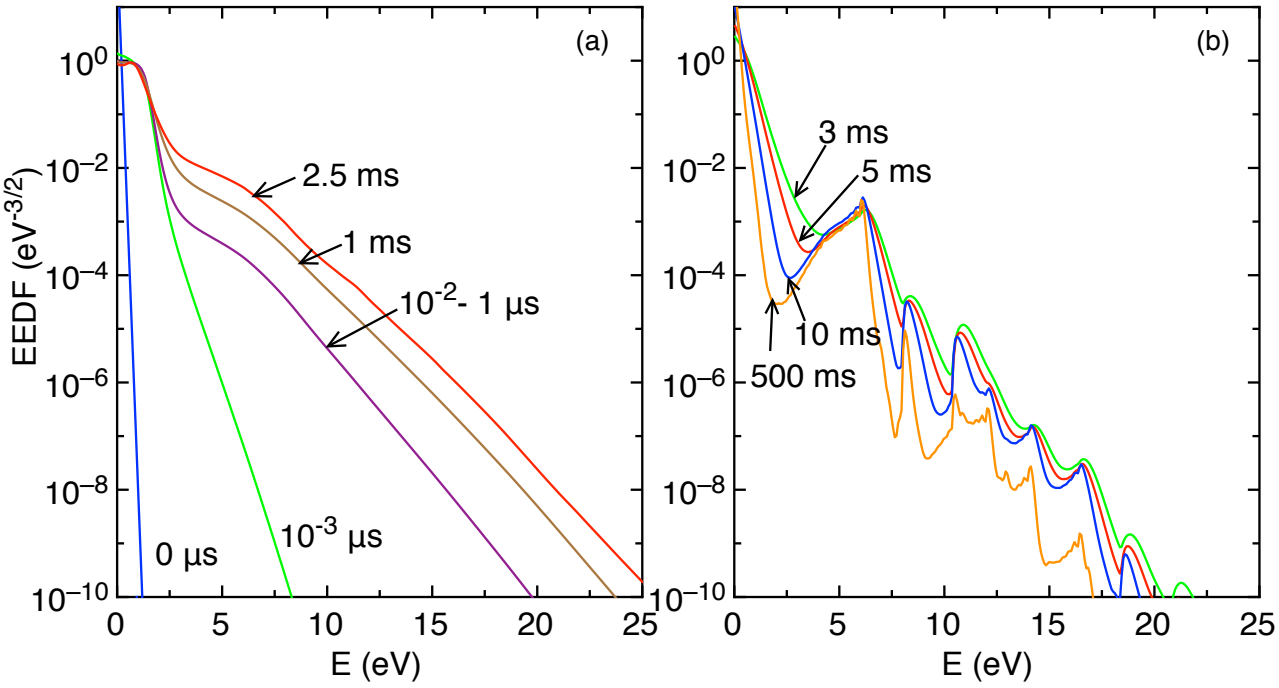

Fig. 6 a and b EEDF time evolution in discharge (a) and post-discharge (b) conditions in the MW test case.

During the discharge, the EEDF increases due to the effect of the electric field and reaches very soon (10^{-2} µs) the quasi-stationary distribution. At longer time (t> 1 ms), the eedf still increases due to the effect of superelastic (vibrational) collisions (see eq. 3.1.1), which transfer vibrational excitation to the electrons.
When the pulse is turned off, the EEDF cools down quickly showing, as in the case of CO_2 [8-10], the characteristic peaks due to superelastic processes involving the metastable electronic excited states $a^3\Pi$, $a'^3\Sigma^+$, $A^1\Pi$, $B^1\Sigma^+$

$$e(\varepsilon) + CO(a^3\Pi) \rightarrow e(\varepsilon + \Delta\varepsilon_1 = 6\ eV) + CO \qquad (3.1.2)$$

$$e(\varepsilon) + CO(a'^3\Sigma) \rightarrow e(\varepsilon + \Delta\varepsilon_2 = 6.8\,eV) + CO \qquad (3.1.3)$$

$$e(\varepsilon) + CO(A^1\Pi) \rightarrow e(\varepsilon + \Delta\varepsilon_3 = 8.03\,eV) + CO \qquad (3.1.4)$$

$$e(\varepsilon) + CO(B^1\Sigma^+) \rightarrow e\left(\varepsilon + \Delta\varepsilon_4 = 10.78\,eV\right) + CO \qquad (3.1.5)$$

creating several peaks in the EEDF at the corresponding electronic excited state energies, i.e. 6, 6.8, 8 and 10.78 eV. Moreover, each peak appears with the periodicity of such energies, i.e. for the $a^3\Pi$, see also [42, 43])

$$e(\varepsilon + \Delta\varepsilon_1) + CO(a^3\Pi) \rightarrow e(\varepsilon + 2\Delta\varepsilon_1) + CO \qquad (3.1.6)$$

The magnitude of the peaks depends on the concentration of the electronic excited states, which in our model is calculated only by considering electron-impact excitation and de-excitation processes (see Met_{CO} process in Table 1) and certainly overestimated, due to the neglect of deactivation mechanisms, such as quenching processes and radiative processes. The results reported in Fig. 6 a-b characterize a situation where the optical allowed transitions are optically thick and therefore completely reabsorbed.

In Fig. 7 a and b, the PVM and DEM rate coefficients are displayed as a function of time in (a) discharge and (b) post-discharge conditions with the corresponding vibrational temperature values, displayed on the second x-axis. In the figures, we report the upper limit value of PVM ($K_d^{(ulPVM)}$ and $K_d^{(ulPVM)}(all)$), the electron impact dissociation rate coefficient DEM of Cosby cross section and of resonant dissociation cross sections, both from ground ($k_d(0)^C$, $k_d(0)^R$) and by including all the CO vibrational levels (DEM^C and DEM^R), and finally the two PVM dissociation rate coefficients due to direct (PVM_1) and Boudouard one (PVM_2).

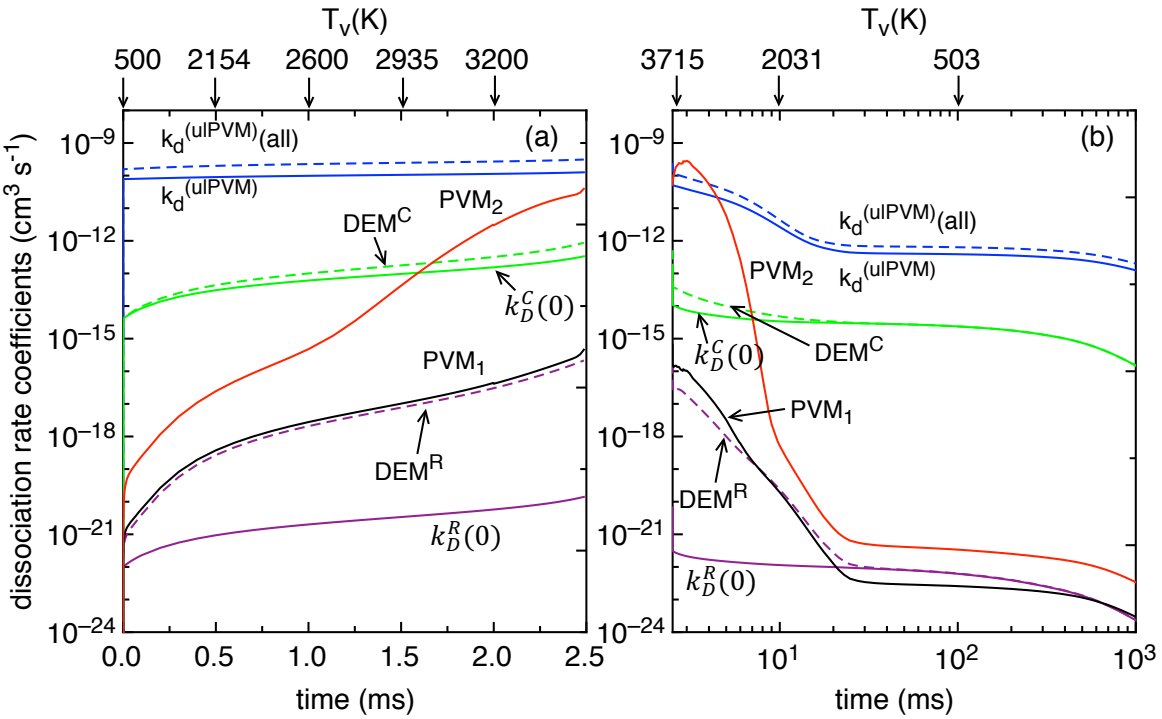

Fig. 7 a and b PVM and DEM rate coefficients as a function of time in discharge (a) and post-discharge (b) in the MW test case. The second x-axis reports the corresponding vibrational temperature values.

The upper limit values of PVM are defined in [8-10] and are proportional to the rate coefficient of e-V resonant vibrational excitation of the transition 0-1 ($K_{eV}(0 \rightarrow 1)$) and 0-v ($K_{eV}(0 \rightarrow v)$)

$$k_d^{(ulPVM)} = \frac{1}{v_{max}} K_{eV}(0 \rightarrow 1) \qquad (3.1.7)$$

$$k_d^{(ulPVM)}(all) = \frac{1}{v_{max}} \sum_v v\, K_{eV}(0 \rightarrow v) \qquad (3.1.8)$$

where v_{max} is the CO maximum quantum vibrational quantum number.
They give an estimation of dissociation rate coefficients induced by vibrational excitation supposing that all the vibrational quanta introduced at the bottom of the vibrational ladder climb up to the dissociation limit without being lost as translational energy (V-T deactivation processes are neglected). DEM rate coefficients from ground state ($k_D^C(0), k_D^R(0)$) instead are calculated by integrating the product of the corresponding electron impact dissociation cross section from ground state (σ_D^C, σ_D^R) with the eedf ($f(\varepsilon)$) over the electron energy axis, i.e

$$k_D^C(0) = \int v(\varepsilon)\sigma_d^C(\varepsilon)f(\varepsilon)d\varepsilon \qquad (3.1.9)$$

$$k_D^R(0) = \int v(\varepsilon)\sigma_d^R(\varepsilon)f(\varepsilon)d\varepsilon \qquad (3.1.10)$$

By including the contribution of dissociation rate coefficients from all the vibrational levels of CO (see process $D_{dir}(v)$ and D_{res} of Table 1), the following more refined DEM rate coefficients can be defined by summing over all the vibrational levels

$$DEM^C = \sum_v k_D^C(v)(E/N,\ f_v, x_{E_i}, x_e, x_C, x_O, x_{C^+}, x_{O^+}) f_v \qquad (3.1.11)$$

$$DEM^R = \sum_v k_D^R(v)\big(E/N,\ f_v, x_{E_i}, x_e, x_C, x_O, x_{C^+}, x_{O^+}\big) f_v \qquad (3.1.12)$$

where $k_D^C(v)$ and $k_D^R(v)$ are the rate coefficients for direct and resonant dissociation from the v^{th} level, f_v the VDF, x_{E_i} the concentration of CO electronic excited states, $x_e, x_C, x_O, x_{C^+}, x_{O^+}$ are, respectively, the electron, C, O, C^+ and O^+ molar fractions.
The two PVM rate coefficients for direct dissociation and Boudouard process can be calculated by

$$PVM_1 = \frac{n_{CO}}{n_e} \sum_v k_D^{direct}(v)(\alpha, T_{gas})\ f_v \qquad (3.1.13)$$

$$PVM_2 = \frac{n_{CO}}{n_e} \sum_{v,w} k_D^{Boud}(v,w)(E_a, T_{gas})\ f_v\, f_w \qquad (3.1.14)$$

where $k_D^{direct}(v)$ and $k_D^{Boud}(v,w)$ are the rate coefficients of eq. (2.3.4) and (2.3.5), which depend on the gas temperature and on the α coefficient for the direct dissociation and on the activation energy E_a for the Boudouard process.
The dominant PVM and DEM rate coefficients correspond, respectively, to the Boudouard dissociation mechanism (PVM_2) and to the Cosby electron impact dissociation (DEM^C). Direct heavy particle dissociation (PVM_1) and resonant electron impact dissociation (DEM^R) rate coefficients are much smaller.
Moreover, PVM_2 rate coefficients overcome DEM^C ones for t>1.5 ms (T_v> 3000 K) in discharge and for t>4 ms (T_v> 3000 K) in the post discharge, showing that vibrational excitation due to V-V up pumped VDF can be very important also for the pure CO system.
Finally, it is interesting to note that DEM^R rate coefficient due to electron impact resonant dissociation calculated by taking into account all CO vibrational ladder differs from that one calculated from only the ground state $k_D^R(0)$, the difference strongly increases with the vibrational temperature.
Such behavior is not shown for the DEM^C and the corresponding $k_D^C(0)$ by Cosby. This is due to the fact that resonant dissociation cross sections strongly increase by increasing the vibrational quantum number, while, for our model assumptions, Cosby's ones have only a threshold energy shift with v. This aspect puts in evidence the need of more refined calculations of vibrational-state resolved direct electron impact dissociation cross sections for CO.
Before ending this section, we want to underline that the present results qualitatively reproduce those reported by [19, 20] for discharge conditions characterized by

E/N=60Td, P=5 torr and $n_e=10^{11}cm^{-3}$. Differences up to orders of magnitude are observed for the vibrational distribution of CO mainly due to the activation energy of 6 eV used in these papers.

3.2 Effect of activation energy of the Boudouard process.

In this section, the dependence of VDF, molar fractions and PVM rate coefficients on the activation energy value used for the Boudouard process is investigated.
Fig. 8 a-c show the VDF in the MW test case of sect. 3.1 at the end of the discharge (a) t= 2.5 ms and at two different times during the post-discharge, (b) t= 3 ms and (c) t= 10 ms, calculated by using the different activation energies previously discussed. As expected, a lower activation energy (E_a=6 eV) results in a more deactivated VDF plateau, the reverse being true for the highest used value of 11.6 eV. The E_a=8.3 eV case, instead, is intermediate between the previous two. The corresponding PVM_2 rate coefficients largely depend on the choice of the activation energy, as shown in Fig. 9 a-b.

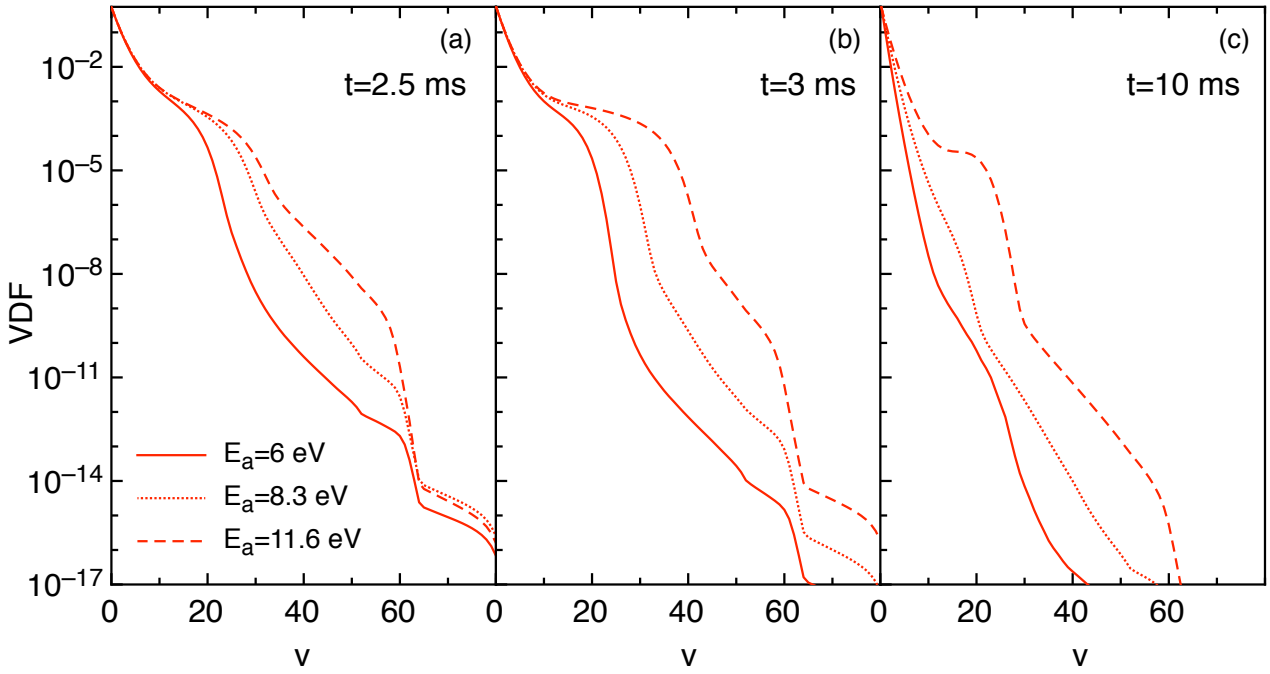

Fig. 8 a-c VDF in the MW test case at three different times (a) t=2.5 ms, (b) t=3 ms, (c) t=10 ms calculated by assuming three different values of the PVM_2 activation energy E_a= 6 eV, 8.3 eV, 11.6 eV

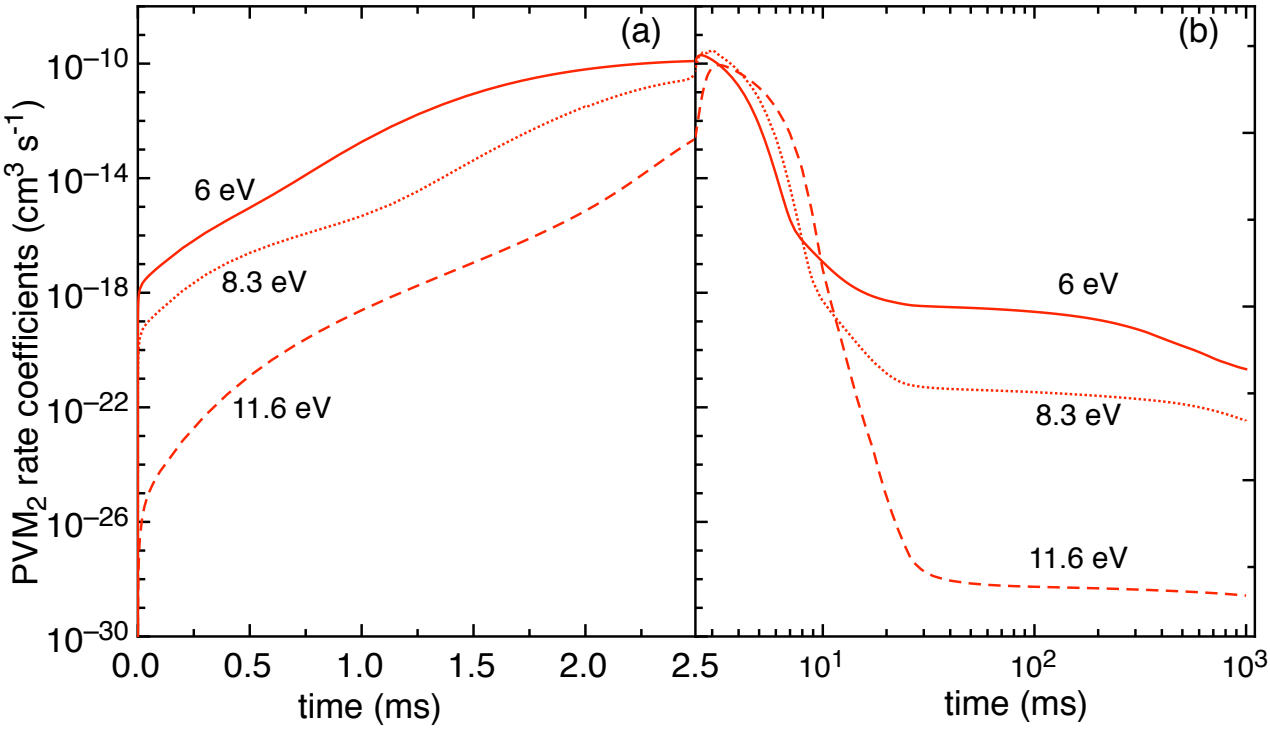

Fig. 9 a-b PVM_2 rate coefficients as a function of time in (a) discharge and (b) post-discharge conditions at the three different values of the PVM_2 activation energy E_a=6, 8.3 and 11.6 eV.

During the discharge phase, lower activation energies result in higher PVM_2 rate coefficients, while in the post discharge regime (Fig. 9 b) the rate coefficients calculated with E_a=6 eV and 8.3 show a similar behavior, being both much higher than the 11.6 eV case. In the early post discharge regime (2.5 ms <t< 3 ms), the rate coefficients depend on the high lying vibrational levels. In particular, a more extended plateau is present in the vdf for E_a=11.6 eV in this temporal regime (see Fig. 8 a-b), causing the temporary increase of the PVM_2 rate coefficients (see Fig. 9 b), although the vibrational temperature, calculated from the first two vibrational levels, is decreasing (see Fig. 4 a).
The PVM_1 rate coefficients, instead, are indirectly affected by the E_a choice only through the corresponding change of the VDF, see eq. (3.1.13).
Fig. 10 a and b show the PVM_1 rate coefficients calculated in (a) discharge and (b) post-discharge conditions at the three E_a values.

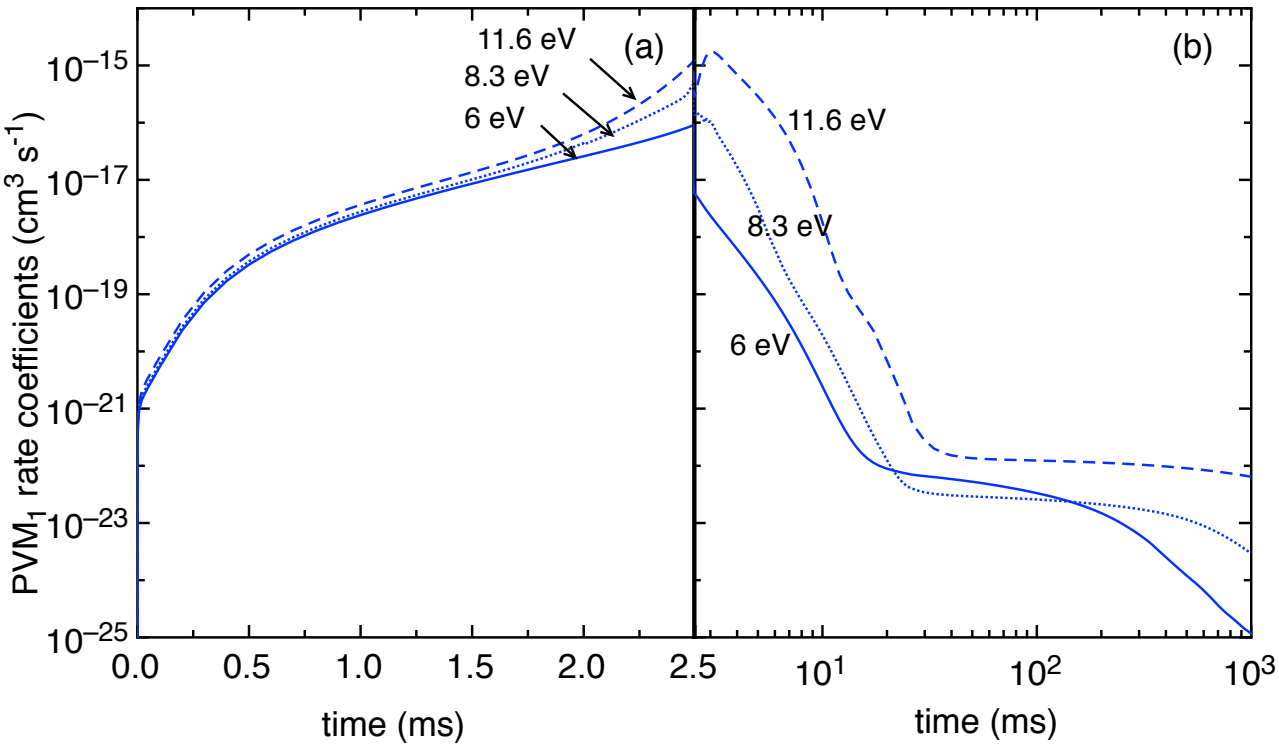

Fig. 10 a and b PVM_1 rate coefficients as a function of time calculated in (a) discharge and (b) post-discharge conditions at the three values of PVM_2 E_a.

Under discharge conditions (Fig. 10 a), the PVM_1 rate coefficients depend on the E_a choice only for the last 0.5 ms of the discharge, i.e. at higher vibrational temperature. A similar behavior is observed in the post discharge conditions (Fig. 10 b) although in this case the dependence of PVM_1 rate coefficients on E_a is much important.
Fig. 11 reports the behavior of the molar fraction on E_a for (a) CO and (b) formed CO_2 as a function of time. The results show the dependence of CO_2 molar fraction on the E_a choice, the 6 eV giving the higher yield. In any case, the maximum of CO_2 is of the order of 10^{-2}, much lower than the corresponding CO molar fraction. This justifies the neglect of the coupling between the vibrational kinetics of CO_2 and CO, that will be necessary in the presence of higher concentrations of CO_2.

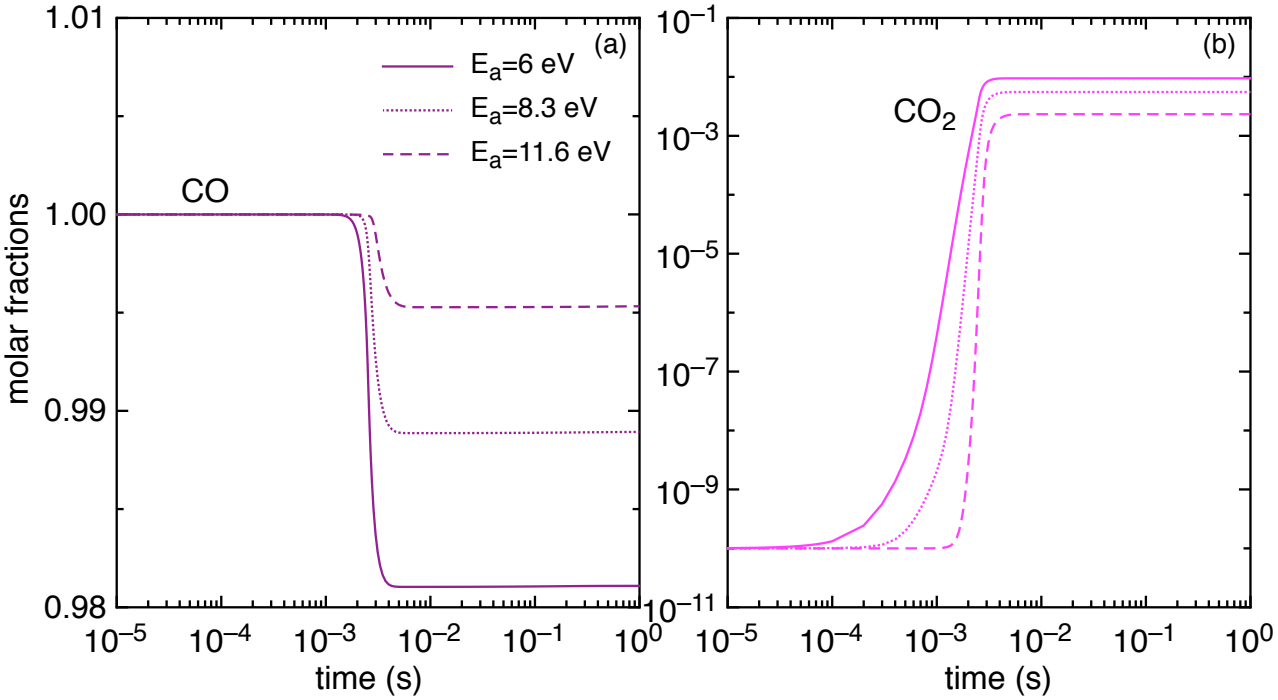

Fig. 11 a and b Time evolution of CO and CO_2 molar fractions calculated by using the three different values of E_a for the PVM_2.

3.3 Effect of gas temperature

Fig. 12 a-d show, respectively, (a) the VDF as a function of v and (b) the PVM_1 and PVM_2 rate coefficients, (c) the DEM and $k_D(0)$ for Cosby and resonant dissociation and (d) the IEM and $k_I(0)$ rate coefficients as a function of $1/T_{gas}$ in the MW test case of sect. 3.1 for different T_{gas} values in the range 500-3000 K. In all the figures, the reported values correspond to the values at the end of the pulse, i.e. t=2.5 ms. The $k_I(0)$ and IEM rate coefficients are obtained as the $k_D(0)$ and DEM ones (see eq. (3.1.9), (3.1.10) and (3.1.11) and (3.1.12)), by substituting the dissociation cross section with the ionization one

$$k_I(0) = \int v(\varepsilon)\sigma_I(\varepsilon)f(\varepsilon)d\varepsilon \qquad (3.3.1)$$

$$IEM = \sum_v k_I(v)(E/N,\ f_v, x_{E_i}, x_e, x_C, x_O, x_{C^+}, x_{O^+})f_v \qquad (3.3.2)$$

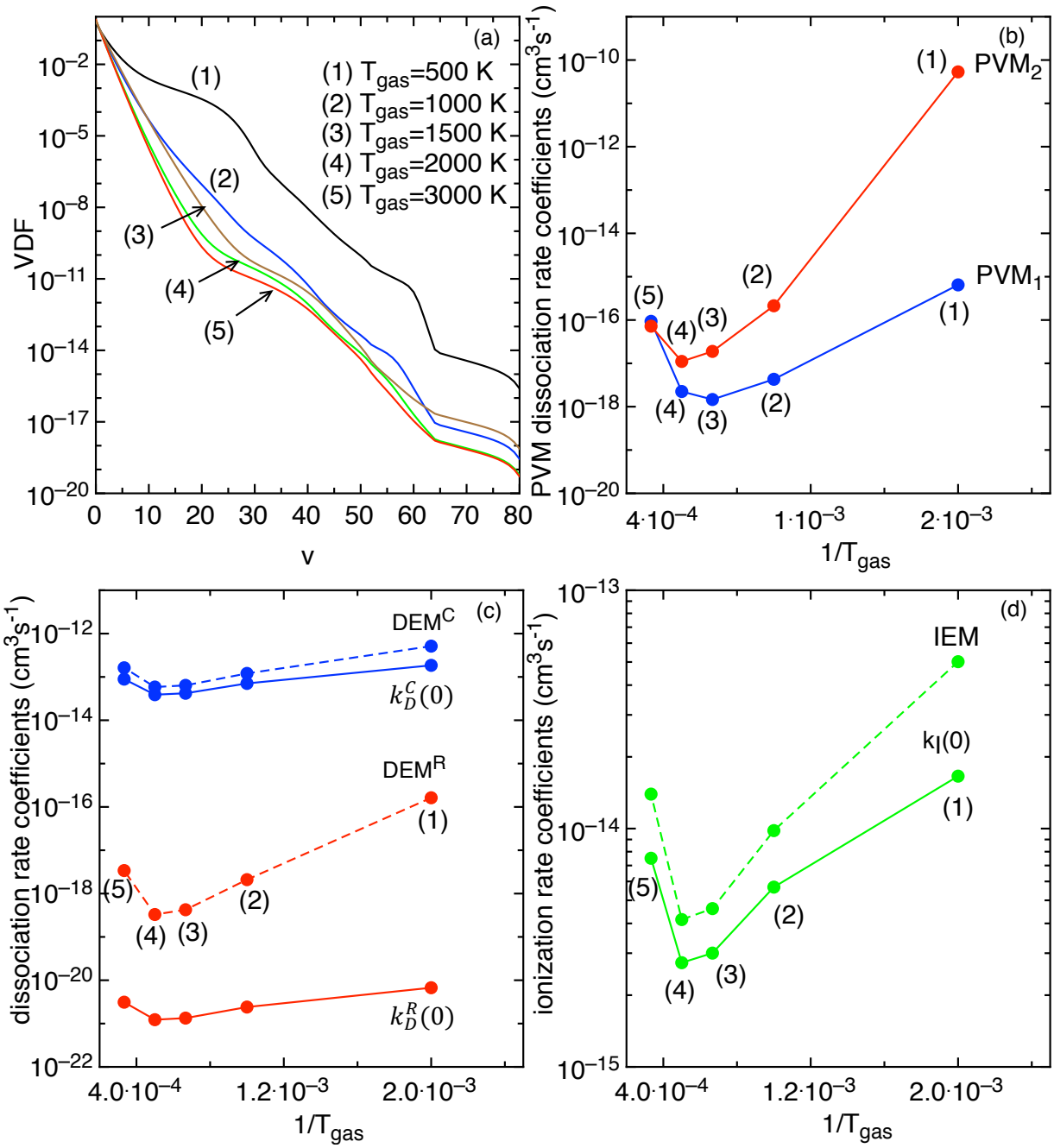

Fig. 12 a-d (a) VDF as a function of v, (b) PVM_1 and PVM_2 rate coefficients, (c) DEM and $k_D(0)$ for Cosby (DEM^C, $k_D^C(0)$) and resonant dissociation (DEM^R, $k_D^R(0)$) and (d) the IEM and $k_I(0)$ rate coefficients as a function of $1/T_{gas}$ for T_{gas} in the range 500-3000 K, in the MW test case.

As shown in Fig. 12 a, the increase of gas temperature depopulates the VDF as a result of the corresponding increase of V-T deactivation rates especially the V-T by C and O atoms as well as of the decrease of the V-V up pumping mechanism. As a consequence, the PVM_1 and PMV_2 rate coefficients present a non-Arrhenius behaviour as a function of $1/T_{gas}$, i.e. the rate coefficients decrease with the increase of the gas temperature, due to the non-equilibrium character of the VDF. The decrease of the plateaux in the reported VDF is not compensated by the

corresponding increase of the rate coefficient. This behaviour was observed also for the pure CO_2 plasma [10]. Only, in the range from 2000 K to 3000K, an increase of PVM_1 and PVM_2 rate coefficients with the increase of T_{gas} is observed, showing an Arrhenius type behavior, since, for T_{gas}>2000 K, the VDF is a quasi-thermal distribution.
Electron impact dissociation rate coefficients (see Fig. 12 c), i.e. $k_D^C(0)$, $k_D^R(0)$, DEM^C, DEM^R (direct and resonant), present a nearly flat trend as a function of $1/T_{gas}$, showing a weak non-Arrhenius behavior as a function of $1/T_{gas}$. This occurs since electron impact dissociation rate coefficients, see for example $k_D^C(v)$ and $k_D^R(v)$ of eq. (3.1.9) and (3.1.10), are only indirectly influenced by the non-equilibrium character of the VDF through the corresponding change in the eedf. The non-Arrhenius character increases especially for resonant dissociation rate coefficients when processes involving vibrationally excited states are included (DEM^R). The ionization rate coefficients $k_I(0)$ and IEM reported in Fig. 12 d present a non-Arrhenius behavior due also to the influence of the E_a choice on the tail of the eedf.
To conclude this section, we want to point out that the increase of gas temperature tends to minimize the V-V up pumping mechanism forming a quasi-Boltzmann vibrational distribution for T>1000 K. This behavior should be present in the microwave discharges operating at atmospheric pressure when high translational gas temperatures can be found (T>2000K).

3.4 Dependence on E/N values

In this section, the dependence of DEM and PVM dissociation rate coefficients on the reduced electric field E/N value is investigated. Fig. 13 a-c show DEM^C (Cosby) and the two PVM rate coefficients as a function of the vibrational temperature for three reduced electric field values, (a) E/N=30 Td, (b) E/N=50 Td and (c) E/N=60 Td. One can note that, only at E/N=60Td, appreciable PVM rate coefficients are obtained. In particular, the PVM_2 ones, always higher than PVM_1, overcome DEM^C from a given vibrational temperature on (see Fig. 13 c). On the other hand, the cases at 30 and 50 Td show a predominance of DEM^C mechanism, because the selected time-pulse (t=2.5 ms) at 30 and 50 Td does not allow a formation of non-equilibrium VDF. Only at the 60 Td case, a well-developed non-equilibrium VDF is created as can be appreciated in Fig. 14, where the VDF is reported as a function of vibrational quantum number for the three values of the electric field, at the end of the pulse. The formation of the plateau is such to increase the PVM_2 rate coefficients, allowing the predominance of this mechanism over the other ones.
For E/N>60 Td, the DEM mechanism should prevail on PVM_2 one because of the corresponding increase of average electron energy, which increases the electron impact dissociation mechanism having less influence on PVM_2 mechanism. In this contest, the E/N value of 60 Td in combination with high vibrational temperatures of CO should be an ideal condition for processes aided by vibrational excitation.

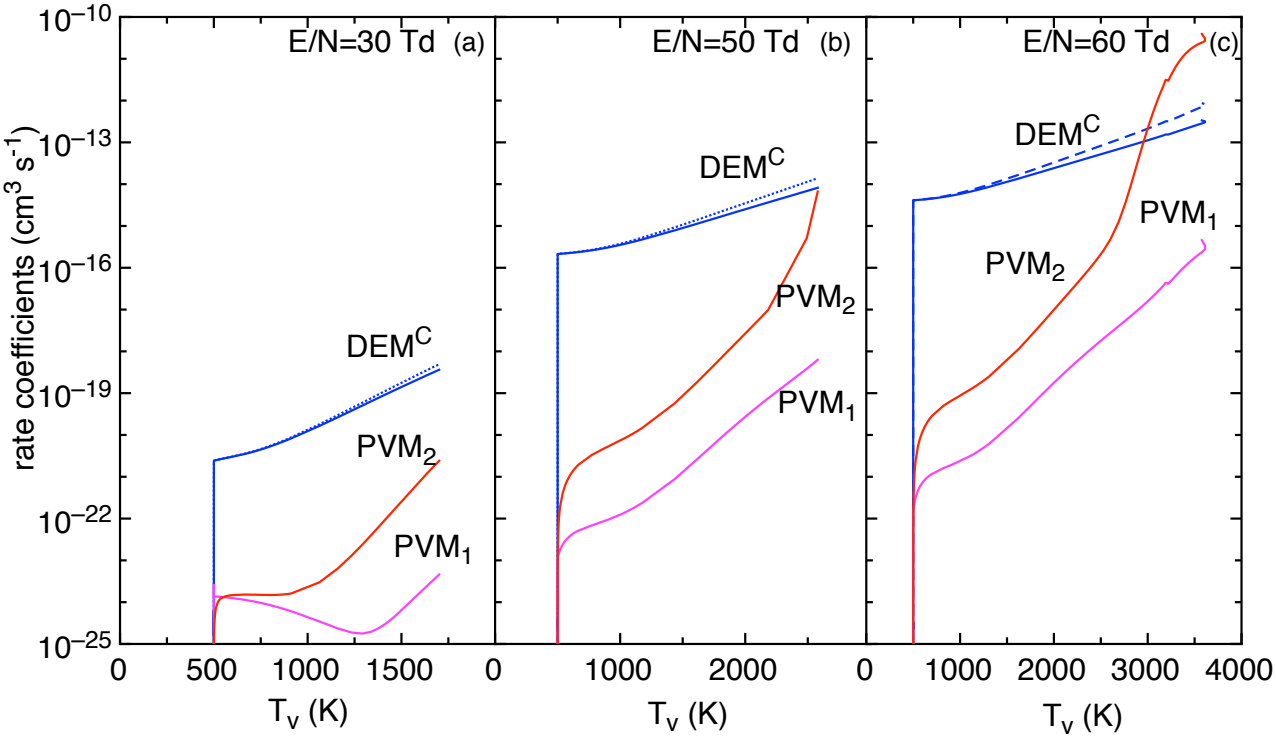

Fig. 13 a-c Electron impact dissociation by Cosby (DEM^C) and pure vibrational mechanism PVM_1 and PVM_2 rate coefficients as a function of the vibrational temperature for different E/N values applied, (a) E/N=30 Td, (b) E/N=50 Td, (c) E/N=60 Td.

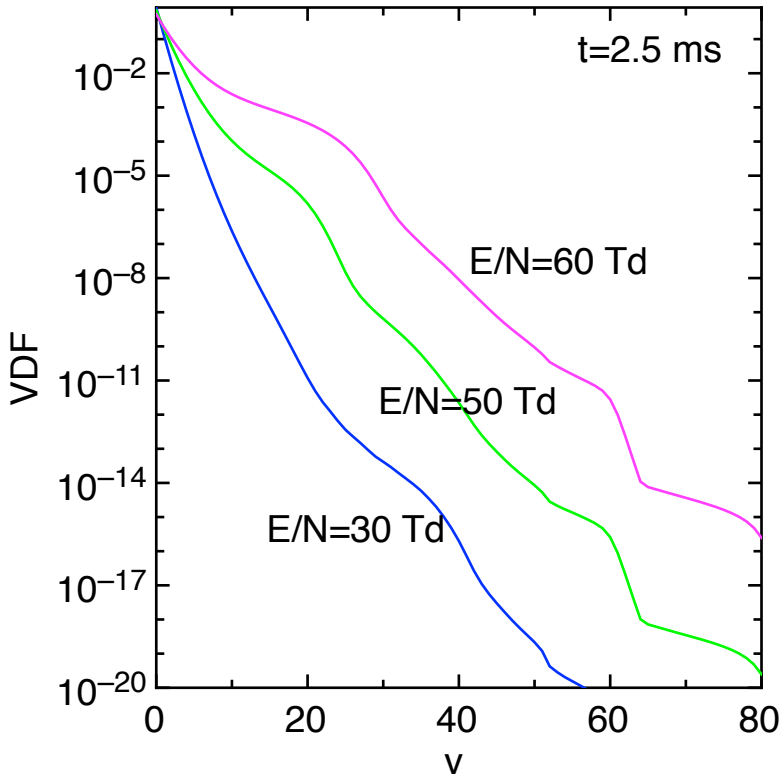

Fig. 14 VDF as a function of v at three different E/N values at the end of the pulse in the MW test case.

3.5 $a^3\Pi$ metastable electronic excited state kinetics

In this section, we discuss an attempt to insert in the present approach a more complete model to describe the kinetics of the $a^3\Pi$ metastable state. To this end, we add to the excitation/deexcitation of the metastable state by electron impact (see also Met_{CO} processes of Table 1)

$$e + CO(0) \leftrightarrow e + CO(a^3\Pi) \qquad (3.5.1)$$

a quenching of the state by heavy particles. During the quenching reaction one can pump vibrational energy in the products according to eqs. (3.5.2) and (3.5.3)

$$CO\left(a^3\Pi,\ \mathrm{w} = 0\right) + CO \rightarrow CO(v = 27) + CO \qquad (3.5.2)\ \text{or}$$

$$CO\left(a^3\Pi,\ \mathrm{w} = 0\right) + CO \rightarrow CO(v = 10) + CO \qquad (3.5.3)$$

Moreover, one can also consider a formation of the metastable through the following reaction

$$CO\left(\mathrm{v} > 27\right) + CO \rightarrow CO\left(a^3\Pi,\ \mathrm{w} = 0\right) + CO \qquad (3.5.4)$$

The rate coefficient of processes (3.5.2) and (3.5.3) has been estimated as $K_{dea}^{a} = 10^{-10} cm^3 s^{-1}$ by [45, 46] with the first experimental measurements of quenching rates. On the other hand, the rate coefficient of the process (3.5.4) has been estimated by $K_{VE}^{a} = 10^{-13} cm^3 s^{-1}$ by [44]. The new kinetic scheme for the $a^3\Pi$ electronic excited state can be written in the following way

$$\frac{dn_{CO(a^3\Pi)}}{dt} = n_e n_{CO(v=0)} k_e^{dir}(0 - a^3\Pi) - n_e n_{CO(a^3\Pi)} k_e^{inv}(0 - a^3\Pi) - n_{CO(a^3\Pi)} n_{CO} K_{dea}^{a} + n_{CO} K_{VE}^{a} \sum_{v>27} n_{CO(v)} \qquad (3.5.5)$$

where $k_e^{dir}(0 - a^3\Pi)$ and $k_e^{inv}(0 - a^3\Pi)$ are the direct and reverse rate coefficients of processes in eq. (3.5.1).

This new kinetic scheme modifies the VDF and to a minor extent the eedf of the CO plasma. In particular, the VDF is strongly affected by the fate of the quenching process in populating the vibrational level of the product (eq. (3.5.2) or (3.5.3)), as it can be appreciated by looking to Fig. 15 a-d, which reports the VDF calculated by considering the kinetic scheme of eq. (3.5.5), including in it the quenching process pumping the v=27 (eq. (3.5.2)), see Fig. 15 a-b, or the v=10 (eq. (3.5.3)), see Fig. 15 c-d. Inspection of the figure shows that the pumping of the v=27 strongly enlarges the VDF with respect to the v=10 case, both in discharge and post-discharge conditions with large effects on the PVM rate coefficients. At the moment, it is very difficult to

decide about the choice of eqs. (3.5.2) and (3.5.3) to be inserted in the vibrational kinetics. Both the possibilities derive by indirect considerations, the v=27 choice can be considered as representing the upper limit of the vibrational pumping through the quenching process, the v=10 level representing a quasi-lower limit.

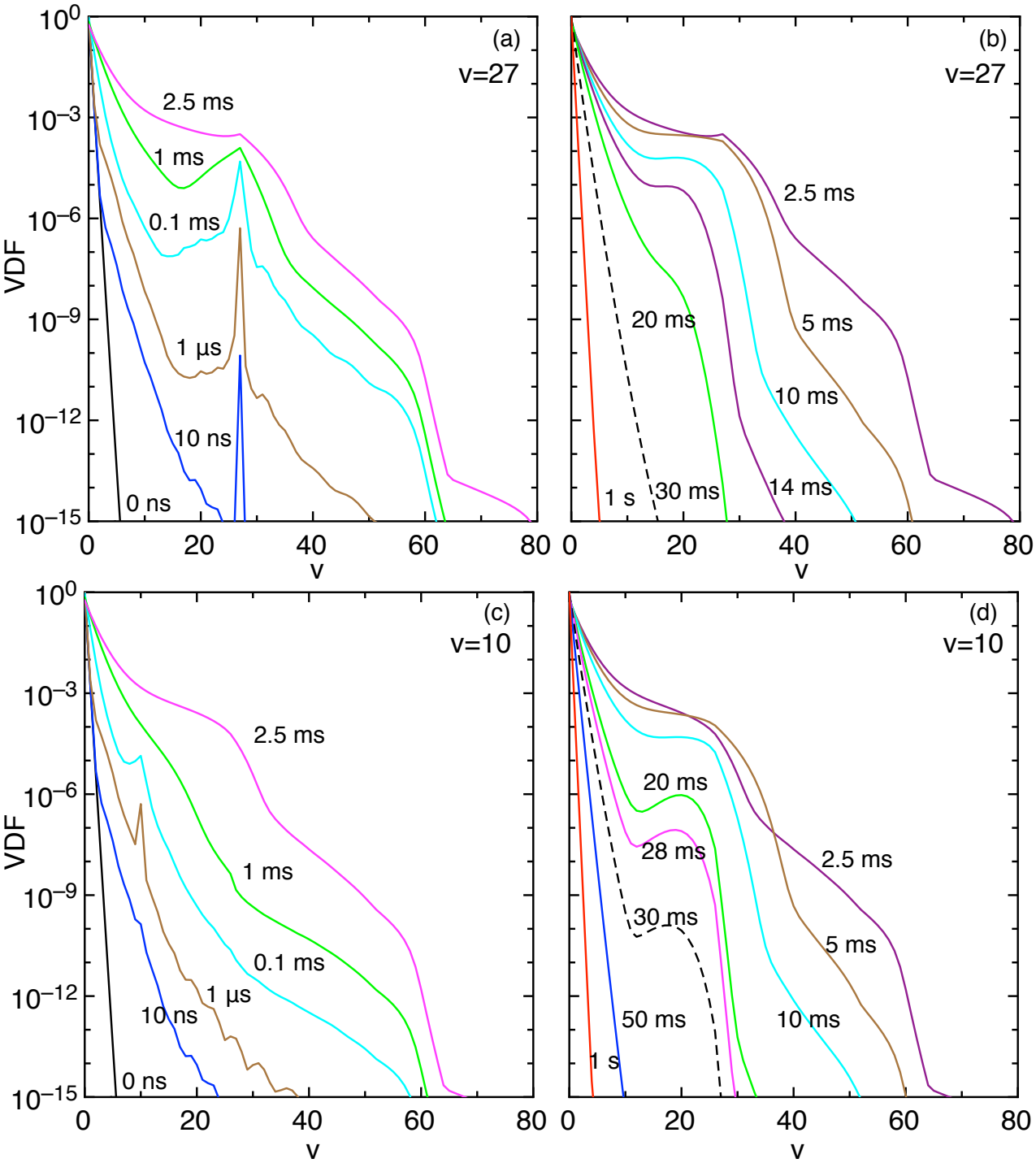

Fig. 15 a-d VDF calculated by considering the kinetic scheme of eq. (3.5.5), by including the quenching process pumping (a-b) the v=27 (eq. (3.5.2)) or (c-d) the v=10 (eq. (3.5.3)), in discharge ((a) and (c)) and post-discharge ((b) and (d)) conditions and by considering E_a=11.6 eV.

4 Conclusions

The results reported in the present paper follow those presented by our group for the CO_2 system, emphasizing the importance of pure vibrational mechanisms in the dissociation of CO competitive with the corresponding DEM ones. Moreover, the role of superelastic electronic and vibrational collisions in affecting eedf under discharge and post discharge conditions results more important than the similar effects found in pure CO_2. All the results indicate the need to consider the kinetics of CO system with the same accuracy of the CO_2, when inserted in the CO_2/CO mixture. As a consequence, future attention should be given to the implementation of the V-V' coupling of CO and CO_2 systems in the whole vibrational ladders.
On the other hand, the introduction of the CO vibrational kinetics into the CO_2 one needs the implementation of a more complete plasma-chemistry model containing also formation and destruction channels of O_2 and C_2 molecules and ions, with O_2 vibrational kinetics. This point should consider an improved kinetics of electronic excited states of CO, O, C, including quenching reactions and optical reabsorption kinetics to better quantify their role in modifying the eedf of CO plasmas [32, 41, 46, 47], as well as the CO_2/CO plasma mixture. Validation of the whole code with experimental results for pure CO_2 and CO systems and their mixtures will become essential for transforming the numerical code in a predictive form useful to indicate the best conditions for the activation of CO/CO_2 species by cold plasmas.

5 Acknowledgement

This work received funding from the project "Apulia Space", PON 03PE-00067.6 from DTA Brindisi (Italy). The authors are very grateful to Prof. Roberto Celiberto and Dr. Vincenzo Laporta for providing the resonant e-V cross sections of CO and Dr. Svetlana Kindysheva for the help in the choice of V-V and V-T rate coefficients for CO+CO collisions.

6 References

[1] Da Silva T, Britun N, Godfroid T and Snyders R 2014 Optical characterization of a microwave pulsed discharge used for dissociation of CO_2 *Plasma Sources Sci. Technol*. **23** 025009
[2] Brehmer F, Welzel S, van de Sanden M C M and Engeln R 2014 CO and byproduct formation during CO_2 reduction in dielectric barrier discharges *J. Appl. Phys*. **116** 123303
[3] Ponduri S, Becher M M, Welzel S, van de Sanden M C M, Loffhagen D and Engeln R 2016 Fluid modelling of CO_2 dissociation in a dielectric barrier discharge *J. Appl. Phys*. **119** 093301
[4] Yao S L, Onyang F, Nekayana A, Suzut E, Oknmoti M and Mizumo A 2000 Oxydative coupling and reforming of methane with carbon dioxide using a high frequency pulsed plasma *Energy Fuels* **14** 910-914

[5] Indarto A, Yang D R, Cho J W, Lee H, Song H K 2007 Gliding arc plasma processing of CO_2 conversion *J Hazard Mater* **146** 309-315
[6] Ramakers M, Trenchev G, Heijkers S, Wang W and Bogaerts A 2017 Gliding arc plasmatron: providing a novel metghod for CO2 conversion *ChemSusChem* **10** 2642-2652
[7] Pietanza L D, Colonna G, D'Ammando G, Laricchiuta A and Capitelli M 2015 Vibrational excitation and dissociation mechanisms of CO_2 under non-equilibrium discharge and post-discharge conditions *Plasma Sources Sci. Technol.* **24** 042002 (Fast Track Communications)
[8] Pietanza L D, Colonna G, D'Ammando G and Capitelli M 2017 Time-dependent coupling of electron energy distribution function, vibrational kinetics of the asymmetric mode of CO_2 and dissociation, ionization and electronic excitation kinetics under discharge and post-discharge conditions *Plasma Phys. Control. Fusion*. **59** 014035
[9] Capitelli M, Colonna G, D'Ammando G, Hassouni K, Laricchiuta A and Pietanza L D 2017 Coupling of plasma chemistry, vibrational kinetics, collisional-radiative models and electron energy distribution function under non-equilibrium conditions *Plasma Process. Polym.* **14** 1600109
[10] Capitelli M, Colonna G, D'Ammando G and Pietanza L D 2017 Self-consistent time dependent vibrational and free electron kinetics for CO_2 dissociation and ionization in cold plasmas *Plasma Sources Sci. Technol*. **26** 055009
[11] Belov I, Vanneste J, Aghaee M, Paulussen S and Bogaerts A Synthesis of micro- and nanomaterials in CO_2 and CO Dielectric Barrier Discharges 2017 *Plasma Process. Polym.* **14** 1600065
[12] Mori S and Suzuki M 2009 Characterization of carbon nanofibers synthesized by microwave plasma-enhanced CVD at low-temperature in a $CO/Ar/O_2$ system *Diam. Rel. Mater.* **18** 678
[13] Kozak T and Bogaerts A 2014 Slitting of CO_2 by vibrational excitation in non-equilibrium plasmas: a reaction kinetics model *Plasma Sources Sci. Technol.* **23** 045004
[14] Kozak T and Bogaerts A 2015 Evaluation of the energy efficiency of CO2 conversion in microwave discharges using a reaction kinetics model *Plasma Sources Sci. Technol.* **24** 015024
[15] Bogaerts A, Wang W, Berthelot A and Guerra V 2016 Modeling plasma-based CO_2 conversion: crucial role of the dissociation cross section *Plasma Sources Sci. Technol.* **25**, 055016
[16] De Benedictis S, Capitelli M, Cramarossa F and Gorse C 1987 Non-equilibrium vibrational kinetics of CO pumped by vibrationally excited nitrogen molecules: a comparison between theory and experiment *Chem. Phys.* **111** 361-370
[17] Essenhigh K A, Utkin Y G, Bernard C, Adamovich I V, Rich J W 2006 Gas-phase Boudouard disproportionation reaction between highly vibrationally excited CO molecules *Chem. Phys.* **330** 506-514
[18] Gorse C, Paniccia F, Bretagne J and Capitelli M 1986 Electron energy distribution functions in Carbon Monoxide discharge and post-discharge conditions:

the role of superelastic electronic collisions from CO($A^3\Pi$) state *J. Appl. Phys.* **59** 731-735
[19] Gorse C, Cacciatore M and Capitelli M 1984 Kinetic processes in non-equilibrium carbon monoxide discharges. I Vibrational kinetics and dissociation rates *Chem. Phys.* **85** 165-176
[20] Gorse C and Capitelli M 1984 Kinetic processes in non-equilibrium carbon monoxide discharges. II Self-consistent electron energy distribution functions, *Chem. Phys.* **85** 177-187
[21] Laporta V, Tennyson J and Celiberto R 2016 Carbon monoxide dissociative attachment and resonant dissociation by electron-impact *Plasma Sources Sci. Technol.* **25** 01LT04
[22] Laporta V, Cassidy C M, Tennyson J and Celiberto R 2012 Electron-impact resonant vibration excitation cross sections and rate coefficients for carbon monoxide *Plasma Sources Sci. Technol.* **21** 045005
[23] Barreto P R, de O. Euclides H, Albernaz A F, Aquilanti V, Capitelli M, Grossi G, Lombardi A, Macheret S and Palazzetti F 2017 Gas phase Bouduard reactions involving singlet-singlet and singlet triplet CO vibrationally excited states: implications for the non-equilibrium vibrational kinetics of CO/CO_2 plasmas *Eur. Phys. J D* submitted
[24] Capitelli M, Dilonardo M and Molinari E 1977 A theoretical calculation of dissociation rates of molecular hydrogen in electrical discharges *Chem. Phys.* **20** 417-429
[25] Colonna G, Tuttafesta M, Capitelli M and Giordano D 1999 Non-Arrhenius NO formation rate in one-dimensional nozzle airflow *J. Thermophys. Heat Transfer* **13** 372-375
[26] Colonna G, Gorse C, Capitelli M, Winkler R and Wilhelm J W 1993 The influence of electron-electron collisions on electron energy distribution functions in N_2 post discharge *Chem. Phys. Lett.* **213** 5-9
[27] Capitelli M, Celiberto R, Colonna G, Esposito F, Gorse C, Hassouni K, Laricchiuta A and Longo S Fundamental aspects of plasma chemical physics, kinetics, Springer Series on Atomic, Optical and Plasma Physics (Springer, New York, 2016)
[28] LXcat database at www.lxcat.net
[29] Itikawa Y 2015 Cross sections for electron collisions with carbon monoxide 2015 *J. Phys. Chem. Ref. Data* **44** 013105; Itikawa database, www.lxcat.net.
[30] P. C. Cosby 1993 Electron-impact dissociation of carbon monoxide *J. Chem. Phys.* **98** 7804
[31] Wang Y, Zatsarinny O and Bartschat K 2013 B-spline R-matrix-with-pseudostates calculations for electron-impact excitation and ionization of carbon, *Phys. Rev. A* **87** 012704; Wang database, www.lxcat.net.
[32] Laher R R and Gilmor F R 2016 Updated Excitation and Ionization Cross Sections for Electron Impact on Atomic Oxygen *J. Phys. Chem. Ref. Data* **19** 277

[33] Macdonald R L, Munafò A, Johnston C O and Panesi M 2016 Nonequilibrium radiation and dissociation of CO molecules in shock-heated flows Phys. Rev. Fluids **1** 043401
[34] Fridman A, *Plasma Chemistry*, Cambrigde University Press, New York (2008)
[35] Plonjes E, Palm P, Chernukho A P, Adamovich I V, Rich J W 2000 Time-resolved Fourier transform infrared spectroscopy of optically pumped carbon monoxide *Chem. Phys.* **256** 315-331
[36] Adamovich I V, Macheret S O, Rich J W and Treanor C E 1998 Vibrational energy transfer rates using a forced harmonic oscillator model *J. Therm. Heat Transf.* **12** 57-65
[37] Cacciatore M and Billing G 1981 Semiclassical calculation of VV and VT rate coefficients in CO *Chem. Phys.* 58 395-407
[38] Schmailzl U and Capitelli M 1979 Nonequilibrium dissociation of CO induced by electron-vibration and IR-laser pumping *Chem. Phys.* **41** 143-151
[39] Langhoff S R and Bauschlicher C W 1995 Global dipole moment function for the $X^1\Sigma^+$ ground state of CO *J. Chem. Phys.* **102** 5220-5225
[40] Rusanov V D, Fridman A A and Sholin S V 1977 *Soviet Phys. Doklady* **22** 757
[41] Martin J P, Perrin M Y, Porshnev P I. 2000 CO_2 formation in an optically excited VV up pumping CO flow *Chem. Phys. Lett.* **332** 283-289
[42] Colonna G and Capitelli M 2001 The influence of atomic and molecular metastable states in high-enthalpy nozzle expansion nitrogen flows *J. Phys. D: Appl. Phys.* **34** 1812
[43] D'Ammando G, Colonna G, Capitelli M and Laricchiuta A 2015 Superelastic collisions under low temperature plasma and afterglow conditions: A golden rule to estimate their quantitative effects *Phys. Plasma* 22 034501
[44] Porshnev P I, Wallaart H L, Perrin M Y, Martin J P 1996 Modeling of optical pumping experiments in CO. I. Time-resolved experiments *Chem. Phys.* **213** 111-122
[45] Dunn O, Harteck P and Dondes S 1973 Isotopic enrichment of carbon-13 and oxygen-18 in the ultraviolet photolysis of carbon monoxide *J.Phys.Chem.* **77** 878
[46] Donovan R J and Husain D 1967 *Trans. Faraday Soc*. **63** 2879
[47] Aliat A, Chihaoui A and Kustova E V 2003 Nonequilibrium kinetics of a radiative CO flow behind a shock wave *Phys. Rev. E* **68** 056306
[48] Aliat A, Kustova E V and Chihaoui A 2005 State-to-state reaction rates in gases with vibration–electronic–dissociation coupling: the influence on a radiative shock heated CO flow *Chem. Phys.* **314** 37-47